Hindawi Publishing Corporation
EURASIP Journal on Wireless Communications and Networking
Volume 2009, Article ID 206524, 12 pages
doi:10.1155/2009/206524

Research Article

Turbo Processing for Joint Channel Estimation, Synchronization, and Decoding in Coded MIMO-OFDM Systems

Hung Nguyen-Le,[1] Tho Le-Ngoc,[1] and Chi Chung Ko[2]

[1] *Department of Electrical and Computer Engineering, Faculty of Engineering, McGill University, Montreal, QC, Canada H3A 2K6*
[2] *Department of Electrical and Computer Engineering, National University of Singapore, Singapore 117576*

Correspondence should be addressed to Tho Le-Ngoc, tho.le-ngoc@mcgill.ca

Received 2 July 2008; Revised 11 November 2008; Accepted 25 December 2008

Recommended by Erchin Serpedin

This paper proposes a turbo joint channel estimation, synchronization, and decoding scheme for coded multiple-input multiple-output orthogonal frequency division multiplexing (MIMO-OFDM) systems. The effects of carrier frequency offset (CFO), sampling frequency offset (SFO), and channel impulse responses (CIRs) on the received samples are analyzed and explored to develop the turbo decoding process and vector recursive least squares (RLSs) algorithm for joint CIR, CFO, and SFO tracking. For burst transmission, with initial estimates derived from the preamble, the proposed scheme can operate without the need of pilot tones during the data segment. Simulation results show that the proposed turbo joint channel estimation, synchronization, and decoding scheme offers fast convergence and low mean squared error (MSE) performance over quasistatic Rayleigh multipath fading channels. The proposed scheme can be used in a coded MIMO-OFDM transceiver in the presence of multipath fading, carrier frequency offset, and sampling frequency offset to provide a bit error rate (BER) performance comparable to that in an ideal case of *perfect* synchronization and channel estimation over a wide range of SFO values.

1. Introduction

Coded multiple-input multiple-output orthogonal frequency division multiplexing (MIMO-OFDM) has been intensively explored for broadband communications over multipath-rich, time-invariant frequency-selective channels [1]. Turbo processing has been considered for coded MIMO and MIMO-OFDM systems for performance enhancement [2–5]. In particular, iterative detection and decoding issues in MIMO systems to achieve near-Shannon capacity limit [2] and performance gain [5] were investigated under the assumption of *perfect* channel estimation and synchronization. Taking into account the effects of *imperfect* channel knowledge on the system performance, [4] developed a combined iterative detection/decoding and channel estimation scheme to improve the overall performance of MIMO-OFDM systems with *perfect* synchronization.

Under *imperfect* synchronization conditions, multicarrier transmissions such as OFDM and MIMO-OFDM are highly susceptible to synchronization errors such as carrier frequency offset (CFO) and sampling frequency offset (SFO) [6–11], especially for operation at low signal-to-noise ratio (SNR) regimes in case of high-performance coded systems. Therefore, estimation of frequency offsets (CFO and SFO) and channel impulse responses (CIRs) are of crucial importance in (coded) MIMO-OFDM systems using coherent detection. So far, most studies on the issue have been focused on separate and sequential CFO/SFO and channel estimation [7, 11–14]. More specifically, channel estimation is performed by assuming that perfect synchronization has been established [12–14], even though channel estimation would be degraded by imperfect synchronization and vice versa. In most practical systems (e.g., WiFi, WiMAX), data is transmitted in bursts, and each burst is appended with a preamble that contains *known* training sequences to facilitate the *initial* synchronization and channel estimation. However, the insufficient accuracy of initially estimated CFO, SFO, and channel responses as well as their time variation still require *known* pilot tones inserted in the data segment of the burst to *update* and *enhance* the CFO, SFO, and channel

estimation accuracy in order to maintain the high system performance at the cost of reduced transmission/bandwidth efficiency (due to inserted pilot tones), for example, in the IEEE802.11 [15], 4 *pilot* tones are inserted in every block of 48 *data* tones, representing an overhead of 8.33%.

Since synchronization and channel estimation are mutually related, joint channel estimation and synchronization would provide better performance [10]. Recently, a few algorithms [8, 16–19] have been proposed for the estimation of CIRs and CFO in *uncoded* MIMO-OFDM systems but these algorithms have neglected the SFO effect in their studies. However, the detrimental effect of the SFO (even for a very small SFO) will likely lead to a significant degradation of the OFDM receiver performance even when perfect CIR and CFO knowledge is available [20]. Specifically, the SFO induces a sampling delay that drifts linearly in time over an OFDM symbol [21]. Without any SFO compensation, this delay hampers the OFDM receiver as soon as the product of the relative SFO and the number of subcarriers become comparable to one [9]. Consequently, OFDM receivers become more vulnerable to the SFO effect as the used FFT size increases. For instance, an SFO of 40 ppm can cause a window shift of up to six samples [21] in a burst of 1000 OFDM symbols used in multiband OFDM systems [22]. As another example, in the presence of sampling clock offset of 1 ppm in the DVB-T 2 K mode [23], the FFT window will move one sample around every 400 symbols [10].

Various SFO, CFO, and channel schemes have been investigated. In [24], a correlation-based SFO estimation scheme for MIMO-OFDM systems in the absence of CFO was proposed. Under the assumption of *perfect* channel estimation, decision-directed (DD) techniques were proposed for joint CFO/SFO estimation and tracking [21] and for phase noise and residual frequency offset compensation [25] in OFDM systems. Unlike [21, 25], under the assumption of *perfect* channel estimation, maximum likelihood (ML-)-based joint CFO and channel estimation schemes using pilot signals in multiuser MIMO-OFDM systems were considered in [18, 19]. An overview of CFO/SFO estimation and compensation schemes using pre-FFT nondata-aided (NDA) acquisition, post-FFT data-aided (DA) acquisition, and post-FFT DA tracking can be found in [6, 26]. However, existing *joint* channel estimation and synchronization algorithms for coded MIMO-OFDM systems have omitted the SFO in their investigations regardless of its detrimental effect [9, 10, 20, 21, 24].

In this paper, we propose a joint synchronization, channel estimation, and decoding turbo processing scheme for coded MIMO-OFDM systems in the presence of quasistatic multipath channels, CFO, and SFO. By analyzing the nonlinear interrelation between CFO, SFO, channel responses, and received subcarriers, we develop an iterative vector recursive least-squares (RLSs-)-based joint CIR, CFO, and SFO tracking scheme that can be incorporated in the turbo processing between the MIMO-demapper and soft-input soft-output (SISO) decoder for the coded MIMO-OFDM receiver. Conceptually, more accurate estimates of CFO, SFO, and CIR can be obtained by using more reliably detected data and also help to enhance the MIMO-demapper output reliability that will improve the performance of the SISO decoder in the next iteration of the turbo process. Furthermore, the use of *soft* estimates alleviates the detrimental effect of error propagation that usually occurs when *hard* decisions are used in a feedback tracking loop or in decision-directed modes. As a result, better accuracy in CFO/SFO/CIR *estimation* and *tracking* can be achieved without the need of *overhead* pilot tones, that is, removing significant transmission efficiency loss and enhancing the spectral efficiency. As *initial* values of the CFO, SFO, and CIR play an important role in the convergence of the joint synchronization, channel estimation, and decoding turbo processing, we also develop a coarse CFO, SFO, and CIR estimation scheme (that was not studied in [27]) applied to the preamble of the burst and based on the combined CFO-SFO perturbation in order to provide the accurately estimated *initial* values of the CFO, SFO, and CIR.

The rest of the paper is organized as follows. Section 2 describes the coded MIMO-OFDM signal model. Section 3 analyzes the effects of CFO, SFO, and channel responses on the received samples. These interrelations are further explored to develop the turbo joint channel estimation, synchronization, and decoding scheme in Section 4, and the vector RLS-based joint CIR, CFO, and SFO tracking algorithm is delineated in Section 5. Section 6 presents the coarse estimation of the CFO, SFO, and CIR. Simulation results for various scenarios are discussed in Section 7. Finally, Section 8 summarizes the paper.

2. System Model

Figure 1 shows a simplified block diagram of a convolutional-coded MIMO-OFDM transmitter using N_t transmit antennas and M-ary quadrature amplitude modulation (M-QAM). This transmitter architecture is similar to the space-time (ST) bit-interleaved coded modulation (BICM) in [28]. Using a serial-to-parallel (S/P) converter, the input convolutional-encoded bitstream is first split into N_t parallel sequences. Each sequence is further bit-interleaved and then organized as a sequence of Q-bit tuples, $\{\mathbf{d}^u_{m,k}\}$, where $Q = \log_2 M$, $u = 1, \ldots, N_t$, and each Q-bit tuple, $\mathbf{d}^u_{m,k} = [d^u_{m,k,0} \cdots d^u_{m,k,Q-1}]^T$, is mapped to a complex-valued symbol, $X_{u,m}(k) \in \mathbf{A}$. $\mathbf{A}$ is the M-ary modulation signaling set, and u, m, and k denote the indices of the transmit antenna, OFDM symbol, and subcarrier, respectively. (Notation: Upper and lower case bold symbols are used to denote matrices and column vector, respectively. $(\cdot)^T$ denotes transpose. $(\cdot)^H$ denotes Hermitian transpose. $(\cdot)^*$ stands for conjugation. $E\{\cdot\}$ is expectation operator. $\mathrm{Re}\{\cdot\}$ and $\mathrm{Im}\{\cdot\}$ denote real and imaginary parts, respectively. $\mathbf{I}_N$ is the $N \times N$ identity matrix, $\otimes$ denotes Kronecker product, and $P(\cdot)$ is the probability operator.)

Each OFDM symbol consists of $K < N$ information bearing subcarriers, where N is the size of the fast Fourier transform (FFT) or inverse-FFT (IFFT). After IFFT, cyclic-prefix (CP) insertion and digital-to-analog conversion

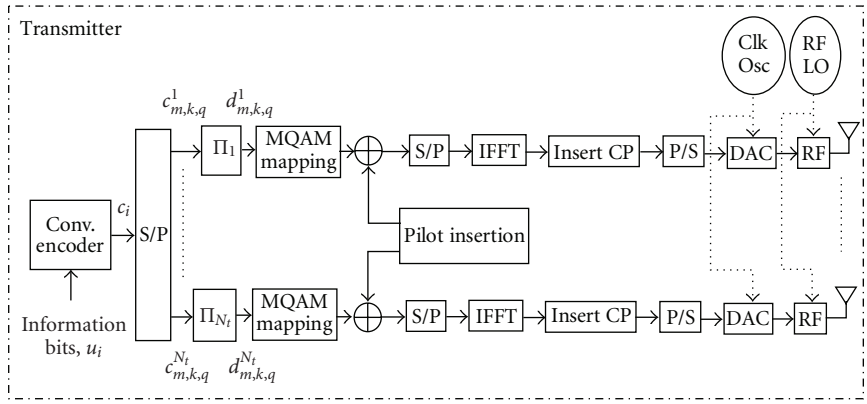

Figure 1: Coded MIMO-OFDM transmitter.

(DAC), the transmitted baseband signal at the uth transmit antenna can be written as

$$s_u(t) = \frac{1}{N} \sum_{m=-\infty}^{+\infty} \sum_{k=-K/2}^{K/2-1} X_{u,m}(k) e^{j(2\pi k/NT)(t-T_g-mT_s)} U(t-mT_s), \tag{1}$$

Where T is the sampling period at the output of IFFT, N_g denotes the number of CP samples, $T_g = N_g T$, $T_s = (N + N_g)T$ is the OFDM symbol length after CP insertion, $u(t)$ is the unit step function, and $U(t) = u(t) - u(t - T_s)$. Practically, the colocated DACs are driven by a common sampling clock with frequency of $1/T$.

The multiple coded OFDM signals are transmitted over a frequency-selective, multipath fading channel. We assume fading conditions are unchanged within an OFDM burst interval, so that the quasistatic channel response between the uth transmit antenna and the vth receive antenna can be represented by

$$h_{u,v}(\tau) = \sum_{l=0}^{L-1} \widetilde{h}_{u,v,l} \delta(\tau - \tau_l), \tag{2}$$

where $\widetilde{h}_{u,v,l}$ and τ_l are the complex gain and delay of the lth path, respectively. L is the total number of resolvable (effective) paths.

3. Effects of CFO, SFO, and Channel Responses on Received Samples

Frequency discrepancies between oscillators used in the radio transmitters and receivers, and channel-induced Doppler shifts cause a *net* carrier frequency offset (CFO) of Δf in the received signal, where f is the operating radio carrier frequency. Practically, it is reasonable to assume that all pairs of transmit-receive antennas experience the same CFO [8], and the received signal at the vth receive antenna element can be written as

$$r_v(t) = e^{j2\pi\Delta f t} \sum_{u=1}^{N_t} \sum_{l=0}^{L-1} \widetilde{h}_{u,v,l} s_u(t - \tau_l) + w_v(t). \tag{3}$$

The impinging signals at all receive antennas are then sampled for analog-to-digital conversion (ADC) by the common receive clock at rate $1/T'$. Since $T' \neq T$, the time alignment of received samples is also affected by the sampling frequency offset (SFO). After sampling and CP removal, the sample of the mth OFDM symbol of the received signal $r_v(t)$ at time instant $t_n = nT'$ is given by

$$r_{v,m,n} = \frac{e^{j(2\pi/N)(N_m+n)\varepsilon_\eta}}{N} \sum_{k=-K/2}^{K/2-1} e^{j(2\pi k/N)n(1+\eta)} e^{j(2\pi k/N)\eta N_m} \times \sum_{u=1}^{N_t} X_{u,m}(k) H_{u,v}(k) + w_{v,m,n}, \tag{4}$$

where $n = 0, 1, \ldots, N-1$, $N_m = N_g + m(N + N_g)$. The complex-valued Gaussian noise sample, $w_{v,m,n}$, has zero mean and a variance of σ^2. $H_{u,v}(k) = \sum_{l=0}^{L-1} h_{u,v,l} e^{-j(2\pi k/N)l}$ is the channel *frequency* response (CFR) at the kth subcarrier for the pair of the uth transmit antenna and the vth receive antenna, and $\mathbf{h}_{u,v} = [\, h_{u,v,0} \;\; h_{u,v,1} \;\; \cdots \;\; h_{u,v,L-1} \,]^T$ is the corresponding effective time-domain channel impulse response (CIR). The SFO and CFO terms are represented in terms of the transmit sampling period T as $\eta = \Delta T/T$, $\Delta T = T' - T$, and $\varepsilon = \Delta f NT = (\Delta f/f)(NTf)$, respectively, and $\varepsilon_\eta = (1 + \eta)\varepsilon$.

As observed in (4), the CFO and SFO induce the time-domain phase rotation that will translate into intercarrier interference (ICI), attenuation, and phase rotation in the frequency domain as shown in the following derivations.

After FFT, the received FD sample at the vth receive antennais $Y_{v,m}(k) = \sum_{n=0}^{N-1} r_{v,m,n} e^{-j(2\pi/N)nk}$. Based on (4), we obtain

$$Y_{v,m}(k) = \sum_{i=-K/2}^{K/2-1} e^{j(2\pi/N)N_m\varepsilon_i} \rho_{i,k} \sum_{u=1}^{N_t} X_{u,m}(i) H_{u,v}(i) + W_{v,m}(k), \tag{5}$$

where $\varepsilon_i = i\eta + \varepsilon_\eta$, $W_{v,m}(k) = \sum_{n=0}^{N-1} w_{v,m}(n + N_m) e^{-j(2\pi/N)nk}$, the ICI coefficient $\rho_{i,k} = (1/N) \sum_{n=0}^{N-1} e^{j(2\pi/N)n(\varepsilon_i+i-k)} \approx \mathrm{sinc}(\varepsilon_i + i - k) e^{j\pi(\varepsilon_i+i-k)}$, and $\mathrm{sinc}(x) = \sin(\pi x)/(\pi x)$. It is noted that the frequency-domain expression of the received

samples in [6, Equation 37] corresponds to an approximation of (5) for the case of the single-input single-output configuration ($N_t = 1$, $N_r = 1$). In the first summation in (5), the term $i = k$ corresponds to the subcarrier of interest, while the other terms with $i \neq k$ represent ICI. As can be observed from the above expression for $\rho_{i,k}$, the term $\varepsilon_i = i\eta + \varepsilon_\eta$ needs to be removed in order to suppress ICI. Obviously, in an *ideal* case with *zero* SFO and CFO, $\varepsilon_i = 0$, $\rho_{i,k} = 1$ for $i = k$ and $\rho_{i,k} = 0$ (i.e., no ICI) for $i \neq k$. Therefore, $Y_{v,m}(k) = \sum_{u=1}^{N_t} X_{u,m}(k)H_{u,v}(k) + W_{v,m}(k)$, and perfect orthogonality among subcarriers is preserved at the receiver. In addition, the coefficient $\rho_{i,k} \approx \operatorname{sinc}(\varepsilon_i + i - k)e^{j\pi(\varepsilon_i + i - k)}$ quantifies the CFO-SFO-induced attenuation and phase rotation of received subcarriers. Thus, to mitigate ICI and attenuation, the effects of CFO and SFO on the received samples have to be compensated. Hence, the estimates of CFO and SFO are needed to compensate for the detrimental effects (phase rotation) of synchronization errors, while the channel estimates are required for the MIMO demapping as illustrated in Figure 2. More specifically, the CFO and SFO compensations will be performed in the time domain (before FFT implementation at receiver) as described in the following derivations.

Following the same approach in [20], the received time-domain sample in (4) can be multiplied by $\exp[-j2\pi\varepsilon_\eta^c n/N]$ prior to FFT to mitigate ICI as shown in Figure 2, that is,

$$r_{v,m,n}^c = r_{v,m,n}e^{-j(2\pi/N)n\varepsilon_\eta^c}, \tag{6}$$

where $\varepsilon_\eta^c = (1+\eta^c)\varepsilon^c$, ε^c, and η^c are the estimates of CFO and SFO, respectively.

After FFT, the resulting subcarriers at the vth receive antenna are

$$Y_{v,m}^c(k) = \sum_{n=0}^{N-1} r_{v,m,n}^c e^{-j(2\pi/N)nk}. \tag{7}$$

After some manipulation, (7) can be rewritten as

$$Y_{v,m}^c(k) = \sum_{i=-K/2}^{K/2-1} e^{j(2\pi/N)N_m\varepsilon_i}\rho_{i,k}^c \sum_{u=1}^{N_t} X_{u,m}(i)H_{u,v}(i) + W_{v,m}^c(k), \tag{8}$$

where

$$W_{v,m}^c(k) = \sum_{n=0}^{N-1} w_{v,m}(n+N_m)e^{-j(2\pi/N)n(1+\eta^c)\varepsilon^c}e^{-j(2\pi/N)nk},$$
$$\rho_{i,k}^c = \frac{1}{N}\sum_{n=0}^{N-1} e^{j(2\pi/N)n[i\eta+(1+\eta)\varepsilon-(1+\eta^c)\varepsilon^c+i-k]}. \tag{9}$$

Based on (8), the vector representation of the frequency-domain (FD) received samples at all receive antennas can be expressed by

$$\mathbf{Y}_m^c(k) = e^{j(2\pi/N)N_m\varepsilon_k}\rho_{k,k}^c\mathbf{H}(k)\mathbf{X}_m(k) + \widetilde{\mathbf{W}}_m^c(k), \tag{10}$$

where the (u,v)th entry of $\mathbf{H}(k)$ is given by $[\mathbf{H}(k)]_{u,v} = H_{u,v}(k)$. Note that $\widetilde{\mathbf{W}}_m^c(k)$ includes both AWGN and residual ICI parts, $\mathbf{X}_m(k) = [X_{1,m}(k)\cdots X_{N_t,m}(k)]^T$, and each of the complex elements in $\widetilde{\mathbf{W}}_m^c(k)$ has a variance of N_0.

Equation (10) provides an insight of the nonlinear interrelation between CFO, SFO, channel responses, and received subcarriers. It indicates that the estimation of CFO (ε^c), SFO (η^c), and channel responses requires knowledge of subcarrier data $\mathbf{X}_m(k)$, while the decoding of subcarrier data $\mathbf{X}_m(k)$ also needs to know the CFO, SFO, and channel responses in addition to the binary convolutional coding structure in $\mathbf{X}_m(k)$. This interrelation can be exploited to develop a high-performance turbo joint channel estimation, synchronization, and decoding scheme that can mutually enhance the estimation accuracy and decoding reliability in an iterative manner. To reduce the number of estimated parameters for the MIMO channel, it is desired to estimate the channel impulse response $\{h_{u,v,0}, h_{u,v,1}, \ldots, h_{u,v,L-1}\}$ instead of the channel frequency response $H_{u,v}(k)$ as $H_{u,v}(k)$ can be derived from the channel impulse response by a simple Fourier transform. The CFO, SFO, and CIR estimation needs to deal with the nonlinear relation as shown in (10) and will be discussed in Section 5. The development of the turbo processing will be addressed in Section 4.

4. Turbo Joint Channel Estimation, Synchronization, and Decoding

The binary convolutional coding structure in $\mathbf{X}_m(k)$ is used to develop the constituent soft-input soft-output (SISO) decoder (shown in Figure 2) to provide more reliable soft estimates of the coded bits, $P(c;O)$, based on the extrinsic soft-bit information received from the MIMO-demapper, $P(c;I)$, using the computations presented in [29]. $P(c;O)$ are then split into N_t streams and interleaved to form N_t soft-bit estimate streams $P(d_{m,k,q}^u;I)$ that are used as extrinsic information for MIMO demapping and CIR, CFO, and SFO estimation as follows.

The purpose of MIMO-demapper is to compute the *extrinsic* soft bit information:

$$P(d_{m,k,q}^u = b;O) = \frac{P(d_{m,k,q}^u = b \mid \mathbf{Y}_m^c(k), \widehat{\mathbf{H}}(k), \widehat{\varepsilon}, \widehat{\eta})}{P(d_{m,k,q}^u = b;I)}, \tag{11}$$

where $b \in \{0,1\}$, and the letters I and O refer to, respectively, the input and output of the MIMO-demapper. Based on (10), the term $P(d_{m,k,q}^u = b \mid \mathbf{Y}_m^c(k), \widehat{\mathbf{H}}(k), \widehat{\varepsilon}, \widehat{\eta})$ can be determined as

$$P(d_{m,k,q}^u = b \mid \mathbf{Y}_m^c(k), \widehat{\mathbf{H}}(k), \widehat{\varepsilon}, \widehat{\eta}) = \sum_{\mathbf{x}\in\mathbf{X}_{u,m,k,q}^{(b)}} P(\mathbf{X}_m(k) = \mathbf{x} \mid \mathbf{Y}_m^c(k), \widehat{\mathbf{H}}(k), \widehat{\varepsilon}, \widehat{\eta}), \tag{12}$$

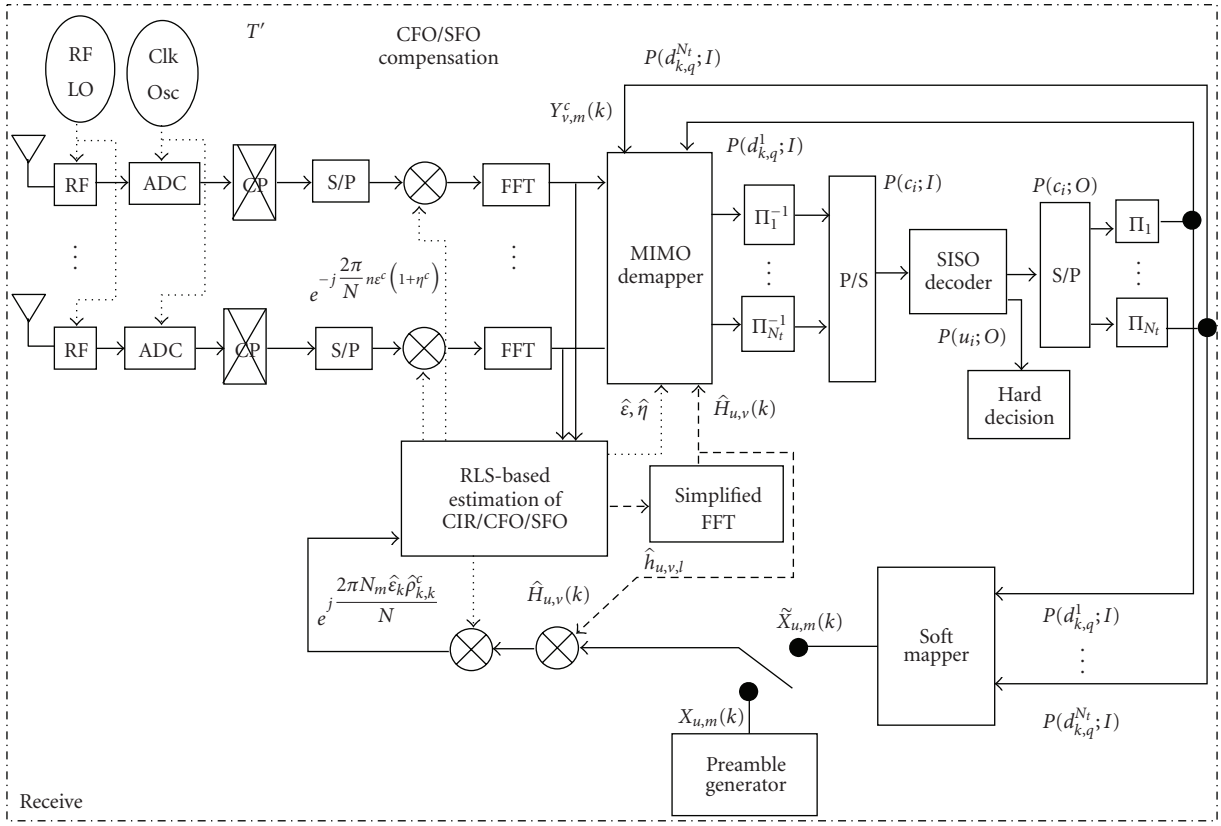

Figure 2: MIMO-OFDM receiver using turbo joint decoding, synchronization, and channel estimation.

where $\mathbf{X}_{u,m,k,q}^{(b)}$ is the set of the vectors $\mathbf{X}_m(k) = [X_{1,m}(k) \cdots X_{N_t,m}(k)]^T$ corresponding to $d_{m,k,q}^u = b$,

$$\begin{aligned}
&P(\mathbf{X}_m(k) = \mathbf{x} \mid \mathbf{Y}_m^c(k), \hat{\mathbf{H}}(k), \hat{\varepsilon}, \hat{\eta}) \\
&\quad = P(\mathbf{Y}_m^c(k) \mid \mathbf{X}_m(k) = \mathbf{x}, \hat{\mathbf{H}}(k), \hat{\varepsilon}, \hat{\eta}) \\
&\qquad \times P(\mathbf{X}_m(k) = \mathbf{x}) / P(\mathbf{Y}_m^c(k)), \\
&P(\mathbf{Y}_m^c(k) \mid \mathbf{X}_m(k) = \mathbf{x}, \hat{\mathbf{H}}(k), \hat{\varepsilon}, \hat{\eta}) \\
&\quad = (\pi N_0)^{-N_r} \exp\big(- \| \mathbf{Y}_m^c(k) \\
&\qquad - e^{j(2\pi/N) N_m \hat{\varepsilon}_k} \hat{\rho}_{k,k}^c \hat{\mathbf{H}}(k) \mathbf{x} \|^2 N_o - 1 \big) \\
&P(\mathbf{Y}_m^c(k)) = \sum_{\mathbf{x} \in \tilde{\mathbf{X}}_m} P(\mathbf{Y}_m^c(k) \mid \mathbf{X}_m(k) = \mathbf{x}, \hat{\mathbf{H}}(k), \hat{\varepsilon}, \hat{\eta}) \\
&\qquad \times P(\mathbf{X}_m(k) = \mathbf{x}),
\end{aligned} \tag{13}$$

where $\tilde{\mathbf{X}}_m$ is the set of all possible values of $\mathbf{X}_m(k)$, $P(\mathbf{X}_m(k) = \mathbf{x}) = \Pi_u \Pi_q P(d_{m,k,q}^u = d_{m,k,q}^u(\mathbf{x}); I)$ due to the use of interleaving, and $d_{m,k,q}^u(\mathbf{x})$ denotes the value of the corresponding bit $d_{m,k,q}^u$ in the vector $\mathbf{x}$.

The above equations, (11) and (12), indicate that unlike the cases of *perfect* channel estimation and synchronization in [2] and *perfect* synchronization in [4], the MIMO demapper herein employs the estimated channel responses, CFO and SFO, $\hat{\mathbf{H}}(k), \hat{\varepsilon}, \hat{\eta}$ to derive the extrinsic soft bit information.

The estimation of channel responses, CFO and SFO, $\hat{\mathbf{H}}(k), \hat{\varepsilon}, \hat{\eta}$, is also based on (10) and hence, needs knowledge of subcarrier data $\mathbf{X}_m(k)$. For this, based on the computed $P(\mathbf{X}_m(k) = \mathbf{x})$, the *soft mapper* (shown in Figure 2) generates the soft estimate, $\tilde{\mathbf{X}}_m(k)$, as its mean, that is,

$$\tilde{\mathbf{X}}_m(k) = E[\mathbf{X}_m(k)] = \sum_{\mathbf{x} \in \tilde{\mathbf{X}}_m} \mathbf{x} P(\mathbf{X}_m(k) = \mathbf{x}). \tag{14}$$

Due to the close interaction between the CIR, CFO, and SFO estimates and the MIMO-demapper, the proposed turbo processing is performed in a joint detection estimation manner (as described above) instead of a *serial* fashion (i.e., updating $\hat{\mathbf{H}}(k), \hat{\varepsilon}, \hat{\eta}$ only after a few iterations for simplicity). As shown in Section 6, convergence to the good performance can be achieved with only 2 or 3 iterations.

The N_t extrinsic soft bit information streams, $P(d_{k,q}^u; O)$, $u = 1, \ldots, N_t$, are then deinterleaved and parallel-to-serial converted to form the extrinsic soft bitstream $P(c; I)$ for the constituent soft-input soft-output (SISO) decoder that will provide more reliable soft estimates of the coded bits, $P(c; O)$, for the next iteration. At any iteration, hard decision can be applied on $P(u; O)$ to produce the decoded data bits. The information flow graph of the proposed turbo joint channel estimation, synchronization,

and decoding scheme, shown in Figure 3, illustrates the iterative exchange of the extrinsic information between the constituent functional blocks in the receiver. By using the *known* training sequence $\mathbf{X}_m(k)$ in the preamble segment of a burst, *initial* estimates of CFO and SFO can be accurately obtained by using the conjugate delay correlation property and then used to establish the *initial* CIR estimates by the vector RLS algorithm as discussed in Section 5.

5. Vector RLS-Based Joint Tracking of CIR, CFO, and SFO

Due to the *nonlinear* effects of CFO and SFO on the received samples as shown by (10) in both time and frequency domains, the joint estimation of CIR, CFO, and SFO would require highly complex *nonlinear* estimation techniques. To avoid such complexity, the paper uses Taylor series to approximately linearize the nonlinear estimation problem. In addition, under the assumption that all transmit-receive antenna pairs experience common CFO and SFO values [7, 8, 11], we can develop a fast-convergence, *vector* RLS-based joint CIR, CFO, and SFO estimation and tracking algorithm suitable for MIMO-OFDM receivers as follows.

As previously discussed, to reduce the number of estimated channel parameters, we consider $\mathbf{h}_{u,v} = [h_{u,v,l}, l = 0, 1, \ldots, L-1]^T$ for $u = 1, \ldots, N_t$, $v = 1, \ldots, N_r$ instead of $\mathbf{H}_{u,v} = [H_{u,v}(k), k = 0, 1, \ldots, K]^T$ since usually $L \ll K$. Using the least squares (LS) criterion, our aim is to iteratively estimate the $(2LN_tN_r + 2) \times 1$ parameter vector $\hat{\boldsymbol{\omega}}_i = [\hat{\omega}_{i,0} \;\; \hat{\omega}_{i,1} \;\; \cdots \;\; \hat{\omega}_{i,2LN_tN_r+1}]^T$ at iteration i to minimize the following weighted squared error sum:

$$C(\hat{\boldsymbol{\omega}}_i) = \sum_{p=1}^{i} \lambda^{i-p} \sum_{v=1}^{N_r} |e_{i,p,v}|^2, \tag{15}$$

where λ is the forgetting factor, $p = 1, \ldots, i$ denotes the pth tone index in the set of i tone indices used in this adaptive estimation. The elements of $\hat{\boldsymbol{\omega}}_i$ are

$$\begin{aligned} \hat{\omega}_{i,l+2L(u-1)+2LN_t(v-1)} &= \mathrm{Re}\{\hat{h}^{(i)}_{u,v,l}\}, \\ \hat{\omega}_{i,l+L+2L(u-1)+2LN_t(v-1)} &= \mathrm{Im}\{\hat{h}^{(i)}_{u,v,l}\}, \\ \hat{\omega}_{i,2LN_tN_r} &= \hat{\varepsilon}^{(i)}, \qquad \hat{\omega}_{i,2LN_tN_r+1} = \hat{\eta}^{(i)}, \end{aligned} \tag{16}$$

with $u = 1, \ldots, N_t$, $v = 1, \ldots, N_r$, $l = 0, \ldots, L-1$. From (10), we obtain

$$\begin{aligned} e_{i,p,v} &= Y^c_{v,m_p}(k_p) - f_v(\widetilde{X}_{u,m_p}(k_p), \hat{\boldsymbol{\omega}}_i), \\ f_v(\widetilde{X}_{u,m_p}(k_p), \hat{\boldsymbol{\omega}}_i) &= e^{j(2\pi/N)N_{m_p}\hat{\varepsilon}^{(i)}_{k_p}} \hat{\rho}^c_{k_p} \sum_{u=1}^{N_t} \widetilde{X}_{u,m_p}(k_p) \hat{H}^{(i)}_{u,v}(k_p), \\ \hat{H}^{(i)}_{u,v}(k_p) &= \sum_{l=0}^{L-1} \hat{h}^{(i)}_{u,v,l} e^{-j(2\pi k_p l/N)}, \\ \hat{\varepsilon}^{(i)}_{k_p} &= k_p\hat{\eta}^{(i)} + (1+\hat{\eta}^{(i)})\hat{\varepsilon}^{(i)}, \\ \hat{\rho}^c_{k_p} &= \frac{1}{N}\sum_{n=0}^{N-1} e^{j(2\pi/N)n[k_p\hat{\eta}^{(i)} + (1+\hat{\eta}^{(i)})\hat{\varepsilon}^{(i)} - (1+\eta^c)\varepsilon^c]}. \end{aligned} \tag{17}$$

It is noted that $\widetilde{X}_{u,m_p}(k_p)$ denotes the *soft* estimate of the pth data tone at subcarrier k_p of the m_pth OFDM symbol from the u th transmit antenna.

It is clear that $f_v(\widetilde{X}_{u,m_p}(k_p), \hat{\boldsymbol{\omega}}_i)$ is a nonlinear function of $\hat{\omega}_{i,2LN_tN_r} = \hat{\varepsilon}^{(i)}$ and $\hat{\omega}_{i,2LN_tN_r+1} = \hat{\eta}^{(i)}$. For a sufficiently small error $e_{i,p,v}$, $f_v(\widetilde{X}_{u,m_p}(k_p), \hat{\boldsymbol{\omega}}_i)$ can be approximately represented by the linear terms of its Taylor series, that is, an approximately linear estimation error can be determined by

$$\begin{aligned} e_{i,p,v} \approx\; & Y^c_{v,m_p}(k_p) - \{f_v(\widetilde{X}_{u,m_p}(k_p), \hat{\boldsymbol{\omega}}_{i-1}) \\ & + \nabla f_v^T(\widetilde{X}_{u,m_p}(k_p), \hat{\boldsymbol{\omega}}_{i-1})(\hat{\boldsymbol{\omega}}_i - \hat{\boldsymbol{\omega}}_{i-1})\}. \end{aligned} \tag{18}$$

The gradient vector of $f_v(\widetilde{X}_{u,m_p}(k_p), \hat{\boldsymbol{\omega}}_{i-1})$ corresponding to the vth receive antenna is determined by

$$\begin{aligned} &\nabla f_v(\widetilde{X}_{u,m_p}(k_p), \hat{\omega}_{i-1}) \\ &\quad = \left[\frac{\partial f_v(\widetilde{X}_{u,m_p}(k_p), \hat{\omega}_{i-1})}{\partial \hat{\omega}_{i-1,0}} \cdots \frac{\partial f_v(\widetilde{X}_{u,m_p}(k_p), \hat{\omega}_{i-1})}{\partial \hat{\omega}_{i-1,2LN_tN_r+1}}\right]^T, \end{aligned} \tag{19}$$

where $\partial f_v(\widetilde{X}_{u,m_p}(k_p), \hat{\boldsymbol{\omega}}_i)/\partial\hat{\omega}_{i,l+2L(u-1)+2LN_t(v-1)} = \widetilde{X}_{u,m_p}(k_p) \times e^{-j(2\pi l k_p/N)} e^{j(2\pi/N)N_m\hat{\varepsilon}^{(i)}_{k_p}} \hat{\rho}^c_{k_p}$, $l = 0, \ldots, L-1$,

$$\begin{aligned} &\frac{\partial f_v(\widetilde{X}_{u,m_p}(k_p), \hat{\boldsymbol{\omega}}_i)}{\partial \hat{\omega}_{i,l+L+2L(u-1)+2LN_t(v-1)}} = j\frac{\partial f_v(\widetilde{X}_{u,m_p}(k_p), \hat{\boldsymbol{\omega}}_i)}{\partial \hat{\omega}_{i,l+2L(u-1)+2LN_t(v-1)}} \\ &\frac{\partial f_v(\widetilde{X}_{u,m_p}(k_p), \hat{\boldsymbol{\omega}}_i)}{\partial \hat{\omega}_{i,2LN_tN_r}} = (1+\hat{\eta}^{(i)})\Omega_{i,p,v} \\ &\Omega_{i,p,v} = e^{j(2\pi/N)N_m\hat{\varepsilon}^{(i)}_{k_p}} \left[j\frac{2\pi}{N}N_m\hat{\rho}^c_{k_p} + \frac{1}{N}\sum_{n=0}^{N-1} j\frac{2\pi}{N}n e^{j(2\pi/N)n[\hat{\varepsilon}^{(i)}_{k_p} - \varepsilon^c_\eta]}\right] \\ &\qquad \times \sum_{u=1}^{N_t} \widetilde{X}_{u,m_p}(k_p)\hat{H}^{(i)}_{u,v}(k_p), \\ &\frac{\partial f_v(\widetilde{X}_{u,m_p}(k_p), \hat{\boldsymbol{\omega}}_i)}{\partial \hat{\omega}_{i,2LN_tN_r+1}} = (k_p + \hat{\varepsilon}^{(i)})\Omega_{i,p,v}, \quad u = 1, \ldots, N_t. \end{aligned} \tag{20}$$

Note that for $\rho = 1, \ldots, N_r$ and $\rho \neq v$, $\partial f_v(\widetilde{X}_{u,m_p}(k_p), \hat{\boldsymbol{\omega}}_i)/\partial\hat{\omega}_{i,l+2L(u-1)+2LN_t(\rho-1)} = 0$, $\partial f_v(\widetilde{X}_{u,m_p}(k_p), \hat{\boldsymbol{\omega}}_i)/\partial\hat{\omega}_{i,l+L+2L(u-1)+2LN_t(\rho-1)} = 0$. Subsequently, the vector RLS algorithm [30] can be used to formulate the following vector RLS-based joint CIR, CFO and SFO tracking scheme.

Initialization. $\mathbf{P}_1 = \gamma^{-1}\mathbf{I}_{2LN_rN_t+2}$, where γ is the regularization parameter. (The use of a scaled identity matrix for initialization is mainly for convenience, and a random initialization matrix can also be employed. Since convergence will invariably be attained, but the final converged position will depend on many environmental factors and are unknown, the difference in using the two types of initialization matrices

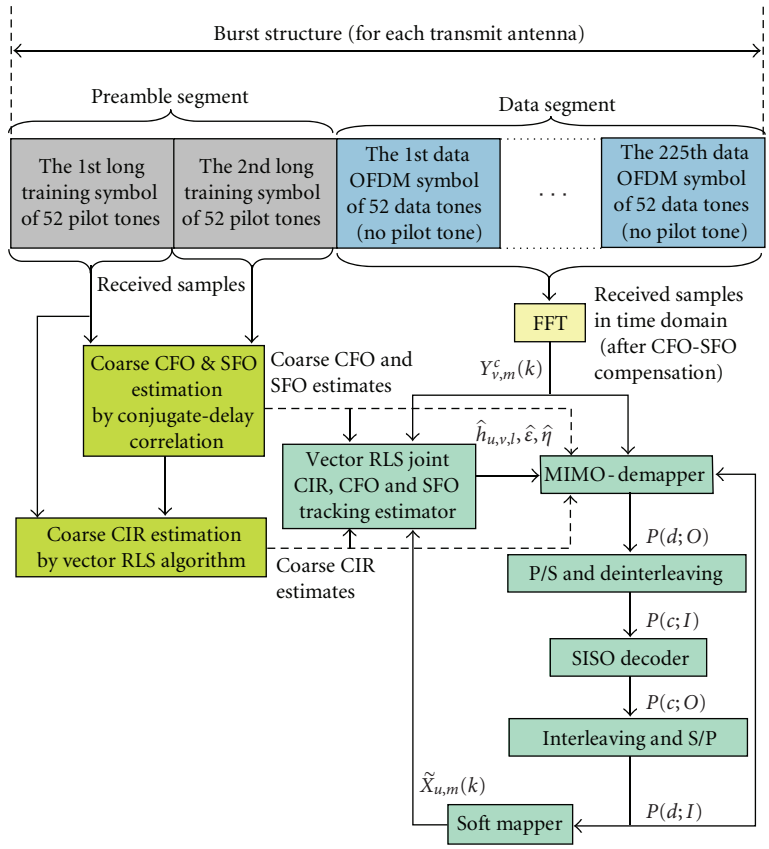

Figure 3: Turbo processing for joint channel estimation, synchronization, and decoding.

is in general not significant. However, due to its randomness, using a random matrix may give rise to problems with matrix inversion or other similar matrix operations under certain conditions. As a result, most adaptive algorithms make use of the more deterministic scaled identity matrix for initialization purposes.)

Iterative Procedure. At the ith iteration with a forgetting factor λ, update

$$\begin{aligned}
&\mathbf{X}_{i,N_r} = \left[\, \nabla f_v^T(\tilde{X}_{u,m_i}(k_i), \hat{\boldsymbol{\omega}}_{i-1}) \;\; \cdots \;\; \nabla f_v^T(\tilde{X}_{u,m_i}(k_i), \hat{\omega}_{i-1}) \,\right],\\
&\mathbf{K}_i = \mathbf{P}_{i-1}\mathbf{X}^*_{i,N_r}\left(\lambda \mathbf{I}_{N_r} + \mathbf{X}^T_{i,N_r}\mathbf{P}_{i-1}\mathbf{X}^*_{i,N_r}\right)^{-1},\\
&\mathbf{P}_i = \lambda^{-1}\left(\mathbf{P}_{i-1} - \mathbf{K}_i\mathbf{X}^T_{i,N_r}\mathbf{P}_{i-1}\right),\\
&\mathbf{e}_{i,N_r} = \left[\left(Y^c_{v,m_i}(k_i) - f_v(\tilde{X}_{u,m_i}(k_i), \hat{\omega}_{i-1})\right), v = 1,\ldots,N_r\right]^T,\\
&\qquad\qquad\qquad\qquad\qquad\qquad u = 1,\ldots,N_t,\\
&\hat{\boldsymbol{\omega}}_i = \hat{\boldsymbol{\omega}}_{i-1} + \mathbf{K}_i\mathbf{e}_{i,N_r}.
\end{aligned} \tag{21}$$

Under the above implementation of the vector RLS-based tracking of CIR, CFO, and SFO algorithm, the resulting computational complexity is $(L^3N_t^3N_r^3N_d)$ per each turbo iteration, where L denotes the channel length, N_t stands for the number of transmit antennas, N_r is the number of receive antennas, and N_d is the number of subcarriers used in each turbo iteration for the vector RLS tracking.

6. Coarse CIR, CFO, and SFO Estimation for Initial Values

For a stationary environment and time-invariant parameter vector, the RLS algorithm is stable regardless of the eigenvalue spread of the input vector correlation matrix [31] as shown in [32]. Due to the use of the first-order Taylor series approximation, the stability of the vector RLS-based CFO, SFO, and CIR tracking scheme requires sufficiently small initial errors between the initial guesses and the true values of CIR, CFO, and SFO.

Accurate yet simple coarse estimation of CFO and SFO can be based on the conjugate delay correlation of the two *identical* and *known* training sequences in the preamble of the burst (as shown in Figure 3), that is, based on (4), we can obtain the following approximation:

$$\begin{aligned}
&E\{r_{v,m_2,n}r^*_{v,m_1,n}\}\\
&\approx \frac{e^{j(2\pi/N)(N+N_g)\varepsilon_\eta}}{N^2}\left|\sum_{k=-K/2}^{K/2-1} e^{j(2\pi k/N)n(1+\eta)}e^{j(2\pi k/N)\eta N_{m_1}} \times\sum_{u=1}^{N_t} X_{u,m_1}(k)H_{u,v}(k)\right|^2,
\end{aligned} \tag{22}$$

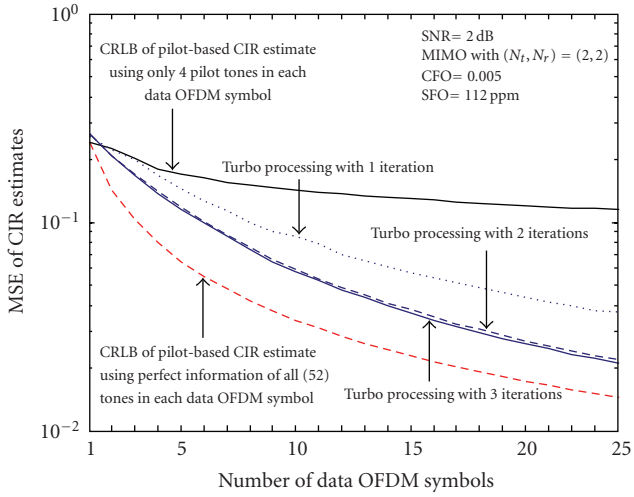

Figure 4: MSE and CRLB of CIR estimates.

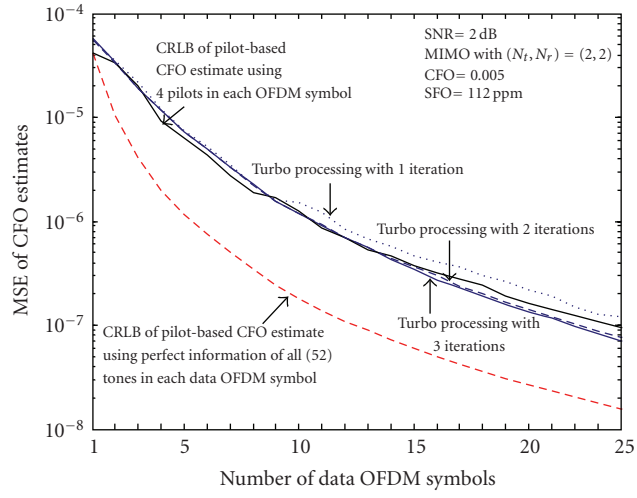

Figure 5: MSE and CRLB of CFO estimates.

where m_1 and $m_2 = m_1 + 1$ denote the indices of the 1st and 2nd training sequences. Therefore, the combined CFO-SFO perturbation can be estimated by

$$\hat{\varepsilon}_\eta = \frac{N}{2\pi(N+N_g)}\Phi[E\{r_{v,m_2,n}r^*_{v,m_1,n}\}], \tag{23}$$

where $\Phi[E\{r_{v,m_2,n}r^*_{v,m_1,n}\}]$ is the angle of $[E\{r_{v,m_2,n}r^*_{v,m_1,n}\}]$.

Under the assumption of $\eta \ll 1$ (e.g., for a typical SFO value of around 50 ppm or 5E-5 in practice) and the use of the two *identical* long training sequences in the preamble of a burst, the coarse (initial) CFO and SFO estimates can be determined separately by

$$\hat{\varepsilon} = \frac{1}{2\pi(N+N_g)N_r}\Phi\left[\sum_{v=1}^{N_r}\sum_{n=0}^{N-1} r_{v,m_2,n}r^*_{v,m_1,n}\right], \quad \hat{\eta} = 0, \tag{24}$$

where $\Phi[\sum_{v=1}^{N_r}\sum_{n=0}^{N-1} r_{v,m_2,n}r^*_{v,m_1,n}]$ is the angle of $\sum_{v=1}^{N_r}\sum_{n=0}^{N-1} r_{v,m_2,n}r^*_{v,m_1,n}$. The above coarse CFO and SFO estimates are then used in the coarse CIR estimation that employs the vector RLS algorithm with the known $\mathbf{X}_m(k)$'s during the preamble.

7. Simulation Results and Discussions

Computer simulation has been conducted to evaluate the performance of the proposed turbo joint channel estimation, synchronization, and decoding scheme for a convolutional-coded MIMO-OFDM system. In the investigation, the OFDM-related parameters are set to be similar to that given by IEEE standard 802.11a [15]. QPSK is employed for data OFDM symbols, each has 52 data tones. Note that in [15], 4 out of 52 data tones are reserved for known pilot tones to facilitate the CIR, CFO, and SFO tracking, which represents an overhead of 8.33%. For the proposed turbo joint channel estimation, synchronization, and decoding scheme, the entire OFDM symbol can be used for data tones to eliminate

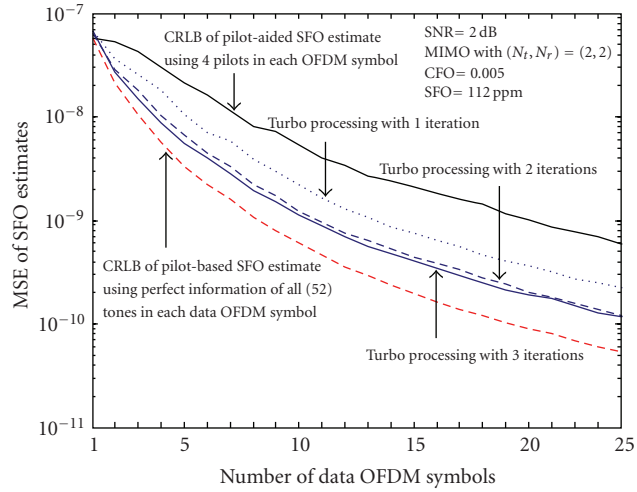

Figure 6: MSE and CRLB of SFO estimates.

this overhead of 8.33%. As illustrated in Figure 3, a burst format of two identical long training symbols and 225 data OFDM symbols was used in the simulation. The two *identical* long training symbols in the preamble of a burst are used to perform a correlation-based coarse CFO-SFO estimation to establish their initial values for the turbo joint tracking of CIR, CFO, and SFO. The *coarse* CIR estimation is performed by using the vector RLS algorithm and the first long training symbols with the available CFO and SFO initial estimates and initial guesses of CIRs and the gradient components at (19) corresponding to CFO-SFO variables set to zeros. The rate 1/2 nonrecursive systematic convolutional code with length covering 2 OFDM symbols is employed for encoding at the transmitter. At the receiver, the SISO decoder is used as discussed in Section 4. For each transmit-receive antenna pair, we consider an exponentially decaying Rayleigh fading channel with a channel length of 5 and a RMS delay spread of 50 nanoseconds. In the simulation, the channel impulse responses and frequency offsets are assumed to be unchanged

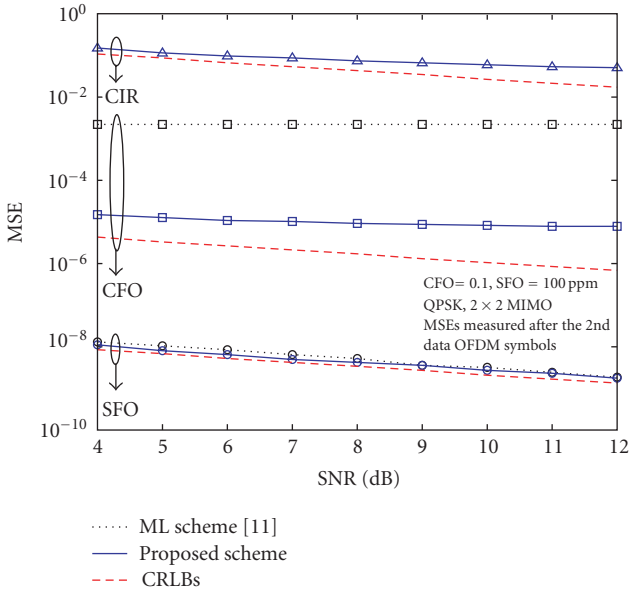

(a) For QPSK

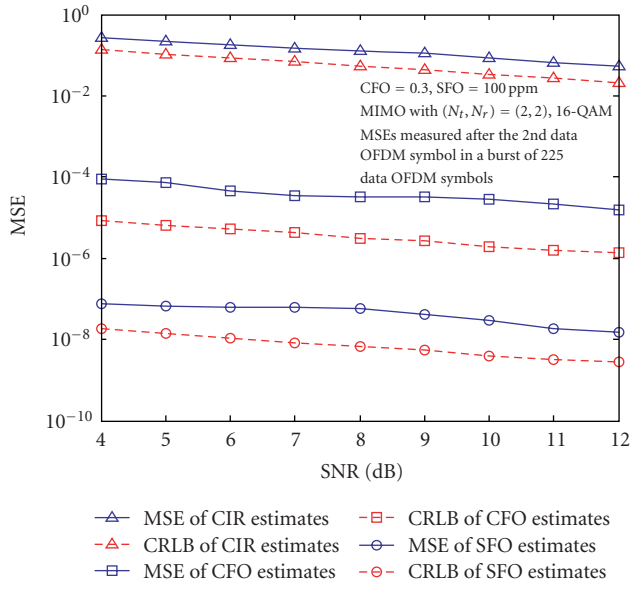

(b) For 16-QAM

Figure 7: MSE and CRLB of CIR, CFO, and SFO estimates versus SNR.

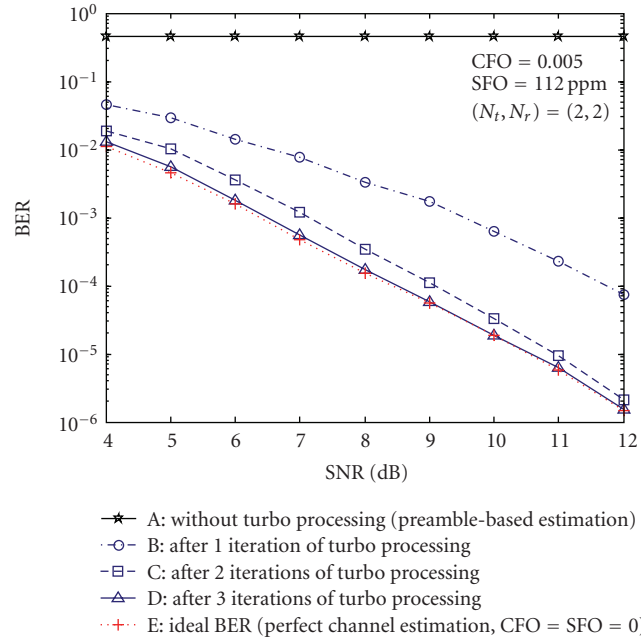

Figure 8: BER performance of the proposed turbo joint channel estimation, synchronization, and decoding scheme.

over the duration of a burst of 227 OFDM symbols (two training OFDM symbols for preamble).

Figure 4 shows the measured mean squared errors (MSEs) of the CIR estimate and relevant Cramér-Rao lower bounds (CRLBs). The numerical results demonstrate that the proposed estimation algorithm provides a fast convergence and the best MSE performance with forgetting factor $\lambda = 1$ and regularization parameter $\gamma = 10$. For comparison, the CRLB values of the CIR estimates obtained by using any unbiased pilot-aided estimation approach with 4 *known* pilot tones (in the IEEE standard 802.11a [15]) and of *all* 52 *known* tones (i.e., ideal but unrealistic case) in each data OFDM symbol are also plotted in Figure 4. As can be seen in Figure 4, the numerical results show that the MSE values of the CIR estimates obtained by the proposed scheme with just one iteration are even smaller than the CRLB obtained by any unbiased pilot-aided joint CIR, CFO, and SFO estimation approach using *4 pilots* in each OFDM symbol. Furthermore, after just 3 iterations, the proposed scheme converges to its best MSE performance close to the CRLB of the ideal but unrealistic case of *all* 52 *known* tones. In the same manner, Figures 5 and 6 show the MSE results and relevant CRLBs of the CFO and SFO estimates, respectively. Figure 7 shows the MSE performance and CRLB values of the proposed turbo scheme with 3 iterations of turbo processing versus SNR for QPSK (a) and 16-QAM (b). As can be seen in Figure 7(a), the proposed joint CIR/CFO/SFO estimation scheme provides more accurate CFO estimates than the existing ML-based CFO and SFO tracking algorithm [11] that requires the use of *perfect channel knowledge*. For the same SNR, the gap between the MSE and corresponding CRLB for QPSK is smaller than that for 16-QAM.

Figure 8 shows the BER performance of the proposed turbo scheme with different numbers of iterations. For reference, the ideal BER performance (curve E) in the case of *perfect* channel estimation and synchronization (i.e., *zero* CFO and SFO, using 3 iterations between MIMO-demapper and SISO decoder) is also plotted. The results show that the performance of the proposed turbo scheme is improved with the number of iterations and can approach that of the case of *perfect* channel estimation and synchronization after 3 iterations (curve D). Without turbo processing, the resulting worst-case BER performance (curve A) corresponding to

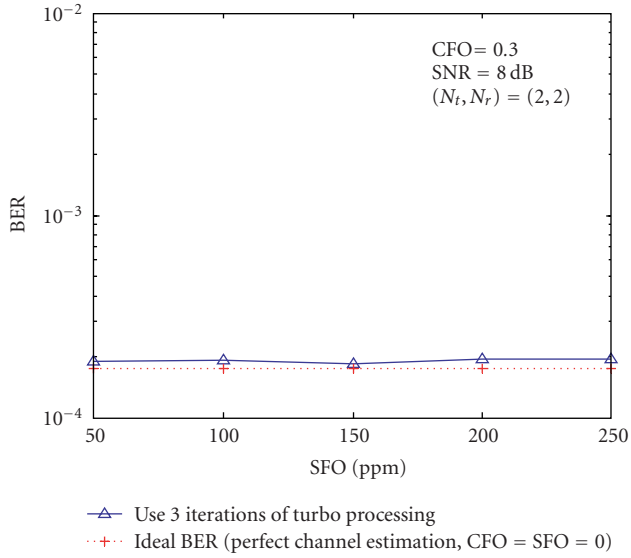

Figure 9: BER performance of the proposed turbo joint channel estimation, synchronization, and decoding scheme under various SFO values.

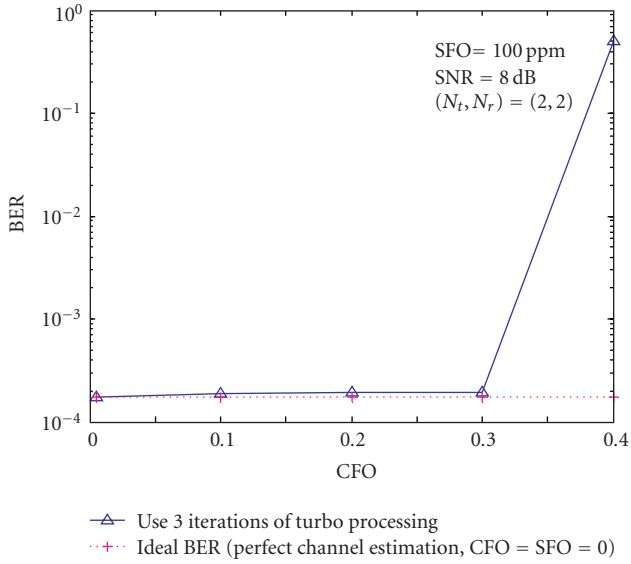

Figure 10: BER performance of the proposed turbo joint channel estimation, synchronization, and decoding scheme under various CFO values.

the case of using only the preamble for the vector RLS-based joint channel estimation and synchronization is plotted in Figure 8. As shown, without the use of the turbo principle, the vector RLS-based joint channel estimation and synchronization scheme using only the preamble (curve A) provides an unacceptable receiver performance (BER values around 0.5), while the proposed turbo scheme offers a remarkable improvement in BER performance even after just one iteration (curve B).

To investigate the effect of CFO and SFO on the performance of the proposed turbo scheme, Figures 9 and 10 show the BER performance of the proposed turbo algorithm under various CFO and SFO values, respectively. For reference, the ideal BER performance in the case of *perfect* channel estimation and synchronization (i.e., *zero* CFO and SFO, using 3 iterations between MIMO-demapper and SISO decoder) is also plotted. As shown, the proposed turbo estimation scheme is highly robust against a wide range of SFO values.

8. Conclusions

In this paper, a received signal model in the presence of CFO, SFO and channel distortions was examined and explored to develop a turbo joint channel estimation, synchronization, and decoding scheme and a vector RLS-based joint CFO, SFO, and CIR tracking algorithm for coded MIMO-OFDM systems over quasistatic Rayleigh multipath fading channels. The astonishing benefits of turbo process enable the proposed joint channel estimation, synchronization, and decoding scheme to provide a near ideal BER performance over a wide range of SFO values without the needs of known pilot tones inserted in the data segment of a burst. Simulation results show that the joint CIR, CFO, and SFO estimation with the turbo principle offers fast convergence and low MSE performance over quasistatic Rayleigh multipath fading channels.

Appendices

A. Cramér-Rao Lower Bound for Pilot-Based Estimates of CIR, CFO, and SFO

Based on (5), the received subcarrier k_i in frequency domain at the vth receive antennacan be expressed by

$$Y_{v,m}(k_i) = e^{j(2\pi/N)N_{m_i}\varepsilon_{k_i}}\rho_{k_i,k_i}\sum_{u=1}^{N_t} X_{u,m}(k_i)H_{u,v}(k_i) + W_{v,m}(k_i). \tag{A.1}$$

Note that ICI components in (A.1) can be assumed to be additive and Gaussian distributed and included in $W_{v,m}(k_i)$ [20].

By collecting K subcarriers in each receive antenna, the resulting KN_r subcarriers from N_r receive antennas can be represented in the vector form as follow:

$$\mathbf{y} = \mathbf{c} + \mathbf{w}, \tag{A.2}$$

where

$$\begin{aligned}\mathbf{y} &= [Y_{1,m_1}(k_1)\cdots Y_{1,m_K}(k_K)\cdots Y_{N_r,m_1}(k_1)\\ &\quad \cdots Y_{N_r,m_K}(k_K)]^T,\\ \mathbf{w} &= [W_{1,m_1}(k_1)\cdots W_{1,m_K}(k_K)\cdots W_{N_r,m_1}(k_1)\\ &\quad \cdots W_{N_r,m_K}(k_K)]^T\\ \mathbf{c} &= (I_{N_r}\otimes(\Phi(\varepsilon,\eta)\mathbf{SF}))\mathbf{h},\end{aligned} \tag{A.3}$$

$$\Phi(\varepsilon,\eta)=\operatorname{diag}\left(e^{j(2\pi/N)N_{m_1}\varepsilon_{k_1}}\rho_{k_1,k_1}\cdots e^{j(2\pi/N)N_{m_K}\varepsilon_{k_K}}\rho_{k_K,k_K}\right),$$

$$\mathbf{S}=\begin{bmatrix}\mathbf{x}(k_1) & 0_{1\times N_t} & 0_{1\times N_t(K-2)}\\ 0_{1\times N_t} & \mathbf{x}(k_2) & 0_{1\times N_t(K-2)}\\ \vdots & \ddots & \vdots\\ 0_{1\times N_t} & 0_{1\times N_t(K-2)} & \mathbf{x}(k_K)\end{bmatrix},$$

$$\mathbf{F}=\begin{bmatrix}\mathbf{F}_1\\ \vdots\\ \mathbf{F}_K\end{bmatrix},\qquad \mathbf{F}_i=\mathbf{I}_{N_t}\otimes\left[1\cdots e^{-j(2\pi/N)(L-1)k_i}\right],$$

$$\mathbf{x}(k_i)=\left[X_1(k_i)\cdots X_{N_t}(k_i)\right],0_{1\times N_t}=\underbrace{[0\cdots 0]}_{N_t\text{ elements}},$$

$$\mathbf{h}=\left[\mathbf{h}_1^T\cdots\mathbf{h}_{N_r}^T\right]^T,$$

$$\mathbf{h}_\nu=\left[h_{1,\nu,0}\cdots h_{1,\nu,L-1}\cdots h_{N_t,\nu,0}\cdots h_{N_t,\nu,L-1}\right]^T,\quad \nu=1,\ldots,N_r \tag{A.4}$$

Based on (A.2), the Fisher information matrix [33] can be computed by

$$\mathbf{M}=\frac{2}{\sigma_w^2}Re\left[\frac{\partial\mathbf{c}^H}{\partial\boldsymbol{\omega}}\frac{\partial\mathbf{c}}{\partial\boldsymbol{\omega}^T}\right], \tag{A.5}$$

where $\boldsymbol{\omega}=[\ \mathbf{h}_R^T\ \ \mathbf{h}_I^T\ \ \varphi^T\ ]^T$, $\mathbf{h}_R=\mathrm{Re}\{\mathbf{h}\}$, $\mathbf{h}_I=\mathrm{Im}\{\mathbf{h}\}$,

$$\varphi=[\ \varepsilon\ \ \eta\ ]^T,$$

$$\frac{\partial\mathbf{c}^H}{\partial\mathbf{h}_R}=\mathbf{I}_{N_r}\otimes\left(\mathbf{F}^H\mathbf{S}^H\Phi^H(\varepsilon,\eta)\right),$$

$$\frac{\partial\mathbf{c}^H}{\partial\mathbf{h}_I}=-j\mathbf{I}_{N_r}\otimes\left(\mathbf{F}^H\mathbf{S}^H\Phi^H(\varepsilon,\eta)\right),$$

$$\frac{\partial\mathbf{c}^H}{\partial\varphi}=\begin{bmatrix}\mathbf{h}^H\left(\mathbf{I}_{N_r}\otimes\left(\mathbf{F}^H\mathbf{S}^H\Phi_\varepsilon^H\right)\right)\\ \mathbf{h}^H\left(\mathbf{I}_{N_r}\otimes\left(\mathbf{F}^H\mathbf{S}^H\Phi_\eta^H\right)\right)\end{bmatrix}, \tag{A.6}$$

$$\frac{\partial\mathbf{c}}{\partial\mathbf{h}_R^T}=\mathbf{I}_{N_r}\otimes\left(\Phi(\varepsilon,\eta)\mathbf{SF}\right),$$

$$\frac{\partial\mathbf{c}}{\partial\mathbf{h}_I^T}=j\mathbf{I}_{N_r}\otimes\left(\Phi(\varepsilon,\eta)\mathbf{SF}\right),$$

$$\frac{\partial\mathbf{c}}{\partial\varphi^T}=\left[\left(\mathbf{I}_{N_r}\otimes\left(\Phi_\varepsilon\mathbf{SF}\right)\right)\mathbf{h}\ \ \left(\mathbf{I}_{N_r}\otimes\left(\Phi_\eta\mathbf{SF}\right)\right)\mathbf{h}\right].$$

Therefore, the Cramér-Rao lower bound of estimated parameters $\boldsymbol{\omega}$, CRLB($\boldsymbol{\omega}$), can be determined by

$$\mathrm{CRLB}(\boldsymbol{\omega})=\operatorname{diag}\left(\mathbf{M}^{-1}\right). \tag{A.7}$$

B. SNR

Based on (4), the signal-to-noise ratio (SNR) at the νth receive antenna is

$$\mathrm{SNR}_\nu=\frac{P_{S,\nu}}{P_N}, \tag{B.1}$$

where

$$P_{S,\nu},=\frac{1}{N^2}E\left\{\left|\sum_{k=-K/2}^{K/2-1}e^{j(2\pi k/N)n(1+\eta)}e^{j(2\pi k/N)\eta N_m}\times\sum_{u=1}^{N_t}X_{u,m}(k)H_{u,\nu}(k)\right|^2\right\}, \tag{B.2}$$

and $P_N=\sigma^2$. Assume that the coefficients of CIR, $\{h_{u,\nu,0},h_{u,\nu,1},\ldots,h_{u,\nu,L-1}\}$, are independent zero-mean complex random variables with common variances$\{\sigma_0^2,\sigma_1^2,\ldots,\sigma_{L-1}^2\}$ for all pairs of transmit-receive antennas, and all receive antennas experience the same AWGN power. After some manipulation, it can be shown that the SNR values at all receive antennas are equal to

$$\mathrm{SNR}=KN_tE_s\sum_{l=0}^{L-1}\frac{\sigma_l^2}{\left(N^2\sigma^2\right)}, \tag{B.3}$$

where $E_s=E\{\,|X_{u,m}(k)|^2\}$ is the average energy of the M-QAM symbols.

Acknowledgment

The authors would like to thank Mr. Robert Morawski for his kind help in running many computer simulations for this paper.

References

[1] H. Bölcskei, "MIMO-OFDM wireless systems: basics, perspectives, and challenges," *IEEE Wireless Communications*, vol. 13, no. 4, pp. 31–37, 2006.

[2] B. M. Hochwald and S. ten Brink, "Achieving near-capacity on a multiple-antenna channel," *IEEE Transactions on Communications*, vol. 51, no. 3, pp. 389–399, 2003.

[3] S. Haykin, M. Sellathurai, Y. de Jong, and T. Willink, "Turbo-MIMO for wireless communications," *IEEE Communications Magazine*, vol. 42, no. 10, pp. 48–53, 2004.

[4] J. Liu and J. Li, "Turbo processing for an OFDM-based MIMO system," *IEEE Transactions on Wireless Communications*, vol. 4, no. 5, pp. 1988–1993, 2005.

[5] P. Liang, S. Feng, Y. Jin, and W. Wu, "A novel turbo MIMO-OFDM system via sequential Monte Carlo," in *Proceedings of the 16th IEEE International Symposium on Personal, Indoor and Mobile Radio Communications (PIMRC '05)*, vol. 2, pp. 984–988, Berlin, Germany, September 2005.

[6] M. Speth, S. A. Fechtel, G. Fock, and H. Meyr, "Optimum receiver design for wireless broad-band systems using OFDM—part I," *IEEE Transactions on Communications*, vol. 47, no. 11, pp. 1668–1677, 1999.

[7] Y. Yao and G. B. Giannakis, "Blind carrier frequency offset estimation in SISO, MIMO, and multiuser OFDM systems," *IEEE Transactions on Communications*, vol. 53, no. 1, pp. 173–183, 2005.

[8] X. Ma, M.-K. Oh, G. B. Giannakis, and D.-J. Park, "Hopping pilots for estimation of frequency-offset and multiantenna channels in MIMO-OFDM," *IEEE Transactions on Communications*, vol. 53, no. 1, pp. 162–172, 2005.

[9] S. Gault, W. Hachem, and P. Ciblat, "Joint sampling clock offset and channel estimation for OFDM signals: Cramér-Rao bound and algorithms," *IEEE Transactions on Signal Processing*, vol. 54, no. 5, pp. 1875–1885, 2006.

[10] B. Ai, Z.-X. Yang, C.-Y. Pan, J.-H. Ge, Y. Wang, and Z. Lu, "On the synchronization techniques for wireless OFDM systems," *IEEE Transactions on Broadcasting*, vol. 52, no. 2, pp. 236–244, 2006.

[11] C. Oberli, "ML-based tracking algorithms for MIMO-OFDM," *IEEE Transactions on Wireless Communications*, vol. 6, no. 7, pp. 2630–2639, 2007.

[12] H. Minn and N. Al-Dhahir, "Optimal training signals for MIMO OFDM channel estimation," *IEEE Transactions on Wireless Communications*, vol. 5, no. 5, pp. 1158–1168, 2006.

[13] M. Cicerone, O. Simeone, and U. Spagnolini, "Channel estimation for MIMO-OFDM systems by modal analysis/filtering," *IEEE Transactions on Communications*, vol. 54, no. 11, pp. 2062–2074, 2006.

[14] Z. J. Wang, Z. Han, and K. J. R. Liu, "A MIMO-OFDM channel estimation approach using time of arrivals," *IEEE Transactions on Wireless Communications*, vol. 4, no. 3, pp. 1207–1213, 2005.

[15] IEEE Computer Society, IEEE Std 802.11a-1999, December 1999.

[16] K. J. Kim and R. A. Iltis, "Frequency offset synchronization and channel estimation for the MIMO-OFDM system using rao-blackwellized gauss-hermite filter," in *Proceedings of IEEE Wireless Communications and Networking Conference (WCNC '06)*, vol. 2, pp. 860–865, Las Vegas, Nev, USA, April 2006.

[17] J. Li, G. Liao, and S. Ouyang, "Jointly tracking dispersive channels and carrier frequency-offset in MIMO-OFDM systems," in *Proceedings of the International Conference on Communications, Circuits and Systems (ICCCAS '06)*, vol. 2, pp. 816–819, Guilin, China, June 2006.

[18] J. Chen, Y.-C. Wu, and T.-S. Ng, "Optimal joint CFO and channel estimation for multiuser MIMO-OFDM systems," in *Proceedings of IEEE International Conference on Communications (ICC '08)*, pp. 563–567, Beijing, China, May 2008.

[19] J. Chen, Y.-C. Wu, S. Ma, and T.-S. Ng, "Joint CFO and channel estimation for multiuser MIMO-OFDM systems with optimal training sequences," *IEEE Transactions on Signal Processing*, vol. 56, no. 8, part 2, pp. 4008–4019, 2008.

[20] H. Nguyen-Le, T. Le-Ngoc, and C. C. Ko, "Joint channel estimation and synchronization with inter-carrier interference reduction for OFDM," in *Proceedings of IEEE International Conference on Communications (ICC '07)*, pp. 2841–2846, Glasgow, Scotland, June 2007.

[21] K. Shi, E. Serpedin, and P. Ciblat, "Decision-directed fine synchronization in OFDM systems," *IEEE Transactions on Communications*, vol. 53, no. 3, pp. 408–412, 2005.

[22] IEEE 802.15-03/268r0, Physical Layer Submission to 802.15 Task Group 3a: Multiband Orthogonal Frequency-Division Multiplexing, 2003.

[23] European Telecommunication Standard ETS 300 744, Digital Broadcasting Systems for Television, Sound and Data Services; Framing Structure, Channel Coding and Modulation for Digital Terrestrial Television, 1996.

[24] Y. Xu, L. Dong, and C. Zhang, "Sampling clock offset estimation algorithm based on IEEE 802.11n," in *Proceedings of IEEE International Conference on Networking, Sensing and Control (ICNSC '08)*, pp. 523–527, Sanya, China, April 2008.

[25] K. Nikitopoulos and A. Polydoros, "Compensation schemes for phase noise and residual frequency offset in OFDM systems," in *Proceedings of IEEE Global Telecommunications Conference (GLOBECOM '01)*, vol. 1, pp. 330–333, San Antonio, Tex, USA, November 2001.

[26] M. Speth, S. Fechtel, G. Fock, and H. Meyr, "Optimum receiver design for OFDM-based broadband transmission—part II: a case study," *IEEE Transactions on Communications*, vol. 49, no. 4, pp. 571–578, 2001.

[27] H. Nguyen-Le, T. Le-Ngoc, and C. C. Ko, "Turbo joint decoding, synchronization and channel estimation for coded MIMO-OFDM systems," in *Proceedings of IEEE International Conference on Communications (ICC '08)*, pp. 4366–4370, Beijing, China, May 2008.

[28] A. M. Tonello, "Space-time bit-interleaved coded modulation with an iterative decoding strategy," in *Proceedings of the 52nd IEEE Vehicular Technology Conference (VTC '00)*, vol. 1, pp. 473–478, Boston, Mass, USA, September 2000.

[29] S. Benedetto, D. Divsalar, G. Montorsi, and F. Pollara, "A soft-input soft-output APP module for iterative decoding of concatenated codes," *IEEE Communications Letters*, vol. 1, no. 1, pp. 22–24, 1997.

[30] J. M. Mendel, *Lessons in Estimation Theory for Signal Processing, Communications, and Control*, Prentice-Hall, Englewood Cliffs, NJ, USA, 1995.

[31] D. G. Manolakis, V. K. Ingle, and S. M. Kogon, *Statistical and Adaptive Signal Processing*, McGraw-Hill, Boston, Mass, USA, 2002.

[32] S. Haykin, *Adaptive Filter Theory*, Prentice-Hall, Englewood Cliffs, NJ, USA, 3rd edition, 1996.

[33] S. M. Kay, *Fundamentals of Statistical Signal Processing*, Prentice-Hall PTR, Englewood Cliffs, NJ, USA, 1998.